Electronic Supplementary Information

Experimental section

Materials: GO, ammonium chloride (NH_4Cl), hydrazine hydrate ($N_2H_4 \cdot H_2O$), sodium hypochlorite (NaClO), sodium hydroxide (NaOH), sodium salicylate ($C_7H_5O_3Na$), sodium sulfate (Na_2SO_4), hydrochloric acid (HCl), ethanol (CH_3CH_2OH), and carbon paper were bought from Beijing Chemical Corporation. Cerium (III) chloride heptahydrate ($CeCl_3 \cdot 7H_2O$, 99%) were obtained from Macklin Chemical Reagent Co, Ltd. Para-(dimethylamino) benzaldehyde ($C_9H_{11}NO$), sodium nitroferricyanide (III) dihydrate ($Na_2Fe(CN)_5NO \cdot 2H_2O$), and Nafion were purchased from Aladdin Ltd. (Shanghai, China). The water used throughout all experiments was purified through a Millipore system.

Preparation of CeO_2-rGO: 10 mL of GO solution (5 mg/mL) was ultrasonically dispersed in 30 mL of 2 M NaOH for 0.5 h. Then 0.5 mmol $CeCl_3 \cdot 7H_2O$ were dissolved in 10 mL water. And the mixture of two solutions was stirred vigorously for 15 min and sealed in a 100 mL Teflon-lined autoclave and maintained at 160 °C for 24 h. The obtained black precipitate was separated by centrifuging, and further washing was done with Millipore water until the supernatant become neutral. Finally, the nanocomposite sample was freeze-dried for 24 h.

Preparation of CeO_2: The synthesis procedures were identical to the above, except that no GO solution was inserted.

Preparation of rGO: The synthesis procedures were identical to the above, except that no $CeCl_3 \cdot 7H_2O$ was inserted.

Preparation of CeO_2+rGO: The CeO_2 and rGO were mixed and grinded for 0.5h.

Preparation of CeO_2-rGO/CP, CeO2/CP, rGO/CP and CeO_2+rGO/CP electrode: 10 mg CeO_2-rGO powders (CeO_2, rGO, CeO_2+rGO) and 40 μL of Nafion solution (5 wt%) were dispersed in 960 μL mixed solution contain 700 μL ethanol and 260 μL H_2O by 1 h sonication to form a homogeneous ink. Then, 10 μL CeO_2-rGO was loaded on a CP with area of 1.0 x 1.0 cm^2 and dried under ambient condition.

Characterizations: XRD patterns were obtained from a Shimazu XRD-6100

diffractometer with Cu Kα radiation (40 kV, 30 mA) of wavelength 0.154 nm (Japan). SEM images were collected from the tungsten lamp-equipped SU3500 scanning electron microscope at an accelerating voltage of 20 kV (HITACHI, Japan). TEM images were obtained from a Zeiss Libra 200FE transmission electron microscope operated at 200 kV. XPS measurements were performed on an ESCALABMK II X-ray photoelectron spectrometer using Mg as the exciting source. The photoluminescence (PL) spectroscopy were recorded on a Shimadzu RF-6000 spectrofluorophotometer. Raman spectroscopy was collected on a Renishaw inVia confocal Raman system. The absorbance data of spectrophotometer were measured on SHIMADZU UV-1800 ultraviolet-visible (UV-Vis) spectrophotometer. The ion chromatography data were collected on Thermofisher ICS 5000 plus using the dual temperature heater, injection valve, conductivity detector, AERS 500 Anions suppressor. (Calibration curve: y=0.152x+0.0042).

Electrochemical measurements: Electrochemical measurements were performed with a CHI 660E electrochemical analyzer (CH Instruments, Inc., Shanghai) using a standard three-electrode system using CeO_2-rGO/CP as the working electrode, graphite rod as the counter electrode, and saturated Ag/AgCl electrode as the reference electrode. In all measurements, saturated Ag/AgCl electrode was calibrated with respect to reversible hydrogen electrode as following: in 0.1 M Na_2SO_4 aqueous solution, E(RHE) = E(Ag/AgCl) + 0.059 × pH + 0.197 V. All experiments were carried out at room temperature. For N_2 reduction experiments, the 0.1 M Na_2SO_4 electrolyte was purged with N_2 for 30 min before the measurement. Potentiostatic test was conducted in N_2-saturated 0.1 M Na_2SO_4 solution in a two-compartment cell, which was separated by Nafion 117 membrane.

Determination of NH_3: The produced NH_3 was detected with indophenol blue by ultraviolet spectroscopy.[1] In detail, 4 mL electrolyte was obatined from the cathodic chamber and mixed with 50 μL oxidizing solution containing NaClO (ρCl = 4 ~ 4.9) and NaOH (0.75 M), 500 μL coloring solution containing 0.4 M $C_7H_5O_3Na$ and 0.32 M NaOH, and 50 μL catalyst solution (1 wt% $Na_2[Fe(CN)_5NO]$) for 2 h. Absorbance measurements were performed at λ = 660 nm. The concentration-absorbance curve

was calibrated using standard NH_4^+ solution with a serious of concentrations. The fitting curve (y = 0.475x + 0.014, R^2 = 0.999) shows good linear relation of absorbance value with NH_4^+ concentration.

Determination of N_2H_4: The N_2H_4 present in the electrolyte was determined by the method of Watt and Chrisp.[2] The mixture of $C_9H_{11}NO$ (5.99 g), HCl (30 mL), and C_2H_5OH (300 mL) was used as a color reagent. In detail, 5 mL electrolyte was removed from the electrochemical reaction vessel, and added into 5 mL above prepared color reagent and stirring 10 min at room temperature. Moreover, the absorbance of the resulting solution was measured at a wavelength of 455 nm. The concentration absorbance curves were calibrated using standard N_2H_4 solution with a series of concentrations. The fitting curve (y = 0.7101x + 0.0431, R^2 = 0.999) shows good linear relation of absorbance value with N_2H_4 concentration.

Calculations of NH_3 yield rate and FE: NH_3 formation rate was calculated using the following equation:

$$NH_3 \text{ yield rate} = [NH_4^+] \times V/(m_{cat.} \times t)$$

FE was calculated according to following equation:

$$FE = 3 \times F \times [NH_4^+] \times V/(18 \times Q)$$

Where $[NH_4^+]$ is the measured NH_4^+ concentration; V is the volume of the cathodic reaction electrolyte; t is the potential applied time; $m_{cat.}$ is the loaded quality of catalyst; F is the Faraday constant; and Q is the quantity of applied electricity

Calculation details： Density functional theory (DFT) + U calculations were performed by using the plane wave-based Vienna ab initio simulation package (VASP).[3-5] The generalized gradient approximation method with Perdew - Burke - Ernzerhof (PBE) functional was used to describe the exchange-correlation interaction among electrons. As suggested by Nolan[6,7] and Gong[8], the Hubbard U value for Ce 4f was set to 5.0 eV. The energy cutoff for the plane wave-basis expansion was set to 400 eV and the atomic relaxation was continued until the forces acting on atoms were smaller than 0.03 eV $Å^{-1}$. The CeO_2 (111) surface was modeled with a 3 × 3 slab in the lateral plane separated by 15 Å of vacuum in between to avoid the interaction between the slab and its period images. The Brillouin zone was sampled with 3 × 3 ×

1 Gamma-center k-point mesh. The free energies of the reaction intermediates were obtained by $\Delta G = \Delta E + \Delta E_{ZPE} - T\Delta S$, where ΔE is the electronic energy difference between the free standing and adsorption states of reaction intermediates, ΔE_{ZPE} is the zero point energy and ΔS is the entropy at 298 K, and the entropies of molecules in the gas phase are obtained from the literature.[9]

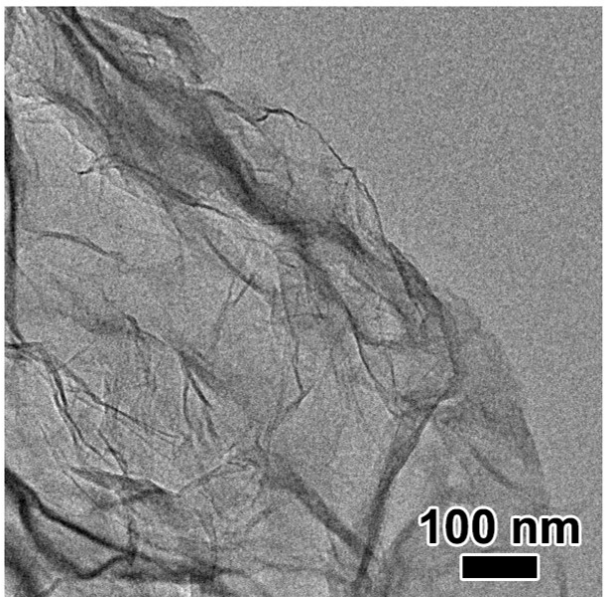

Fig. S1. The TEM image of the rGO.

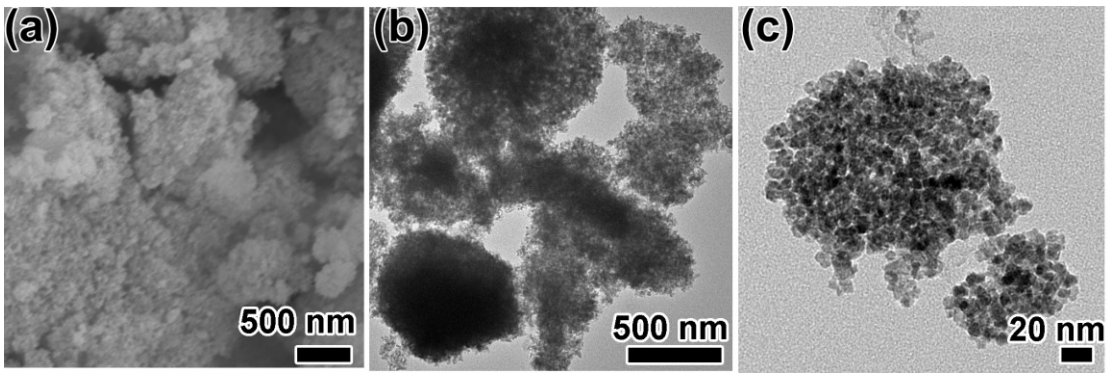

Fig. S2. The SEM (a) and TEM ((b) and (c)) images of the CeO_2.

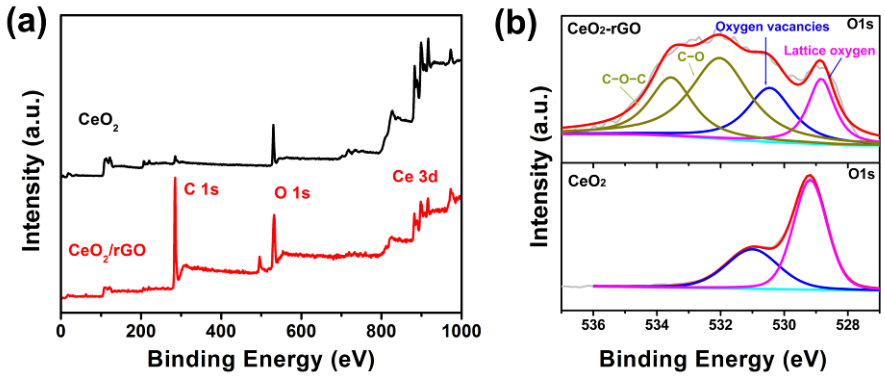

Fig. S3. (a) XPS survey spectra of CeO_2-GO and CeO_2. (b) O 1s XPS spectra of CeO_2-GO and CeO_2

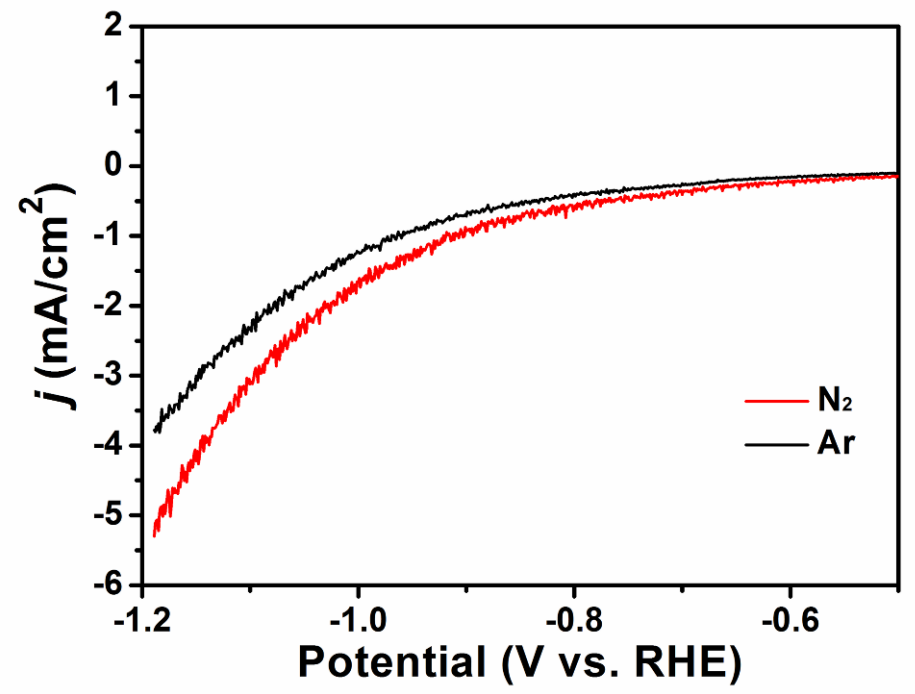

Fig. S4. The linear sweep voltammetric curves using CeO_2-rGO as the working electrode in 0.1 M Na_2SO_4 aqueous solution.

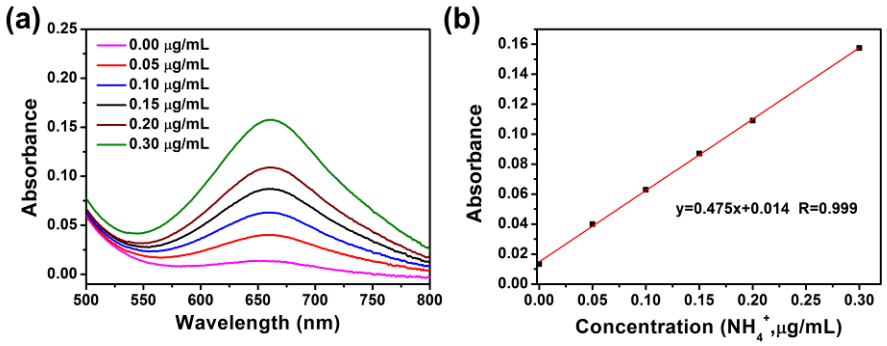

Fig. S5. (a) UV-Vis absorption spectra of indophenol assays with NH_4^+ concentrations after incubated for 2 h at room temperature. (b) Calibration curve used for calculation of NH_4^+ concentrations.

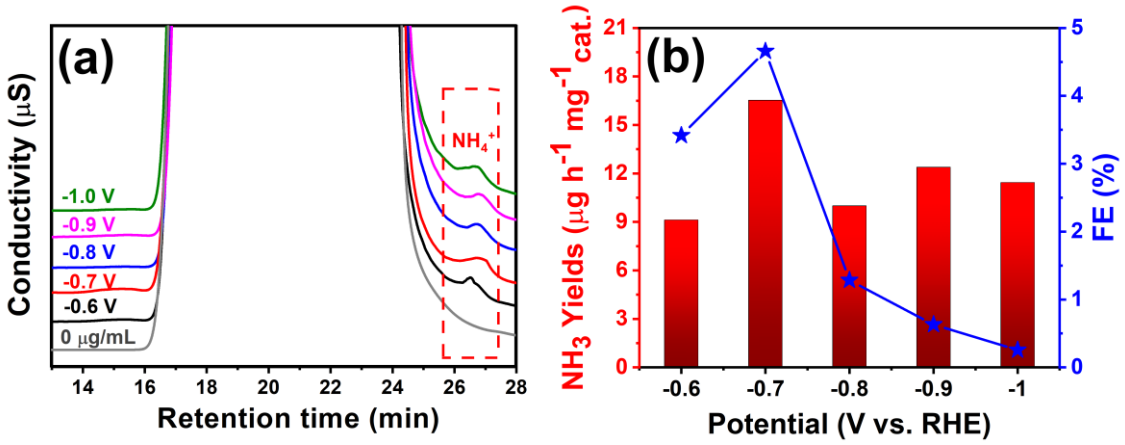

Fig. S6. (a) Ion chromatogram data for the electrolytes at a series of potentials after electrolysis for 2 h. (d) NH_3 yields and FEs for CeO_2-rGO/CP at corresponding potentials.

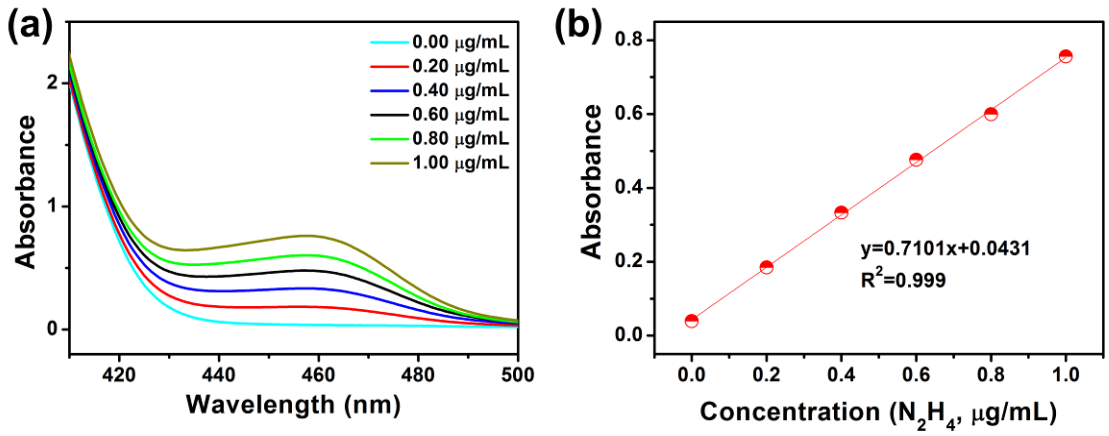

Fig. S7. (a) UV-Vis absorption spectra of various N_2H_4 concentrations after incubated for 10 min at room temperature. (b) Calibration curve used for calculation of N_2H_4 concentrations.

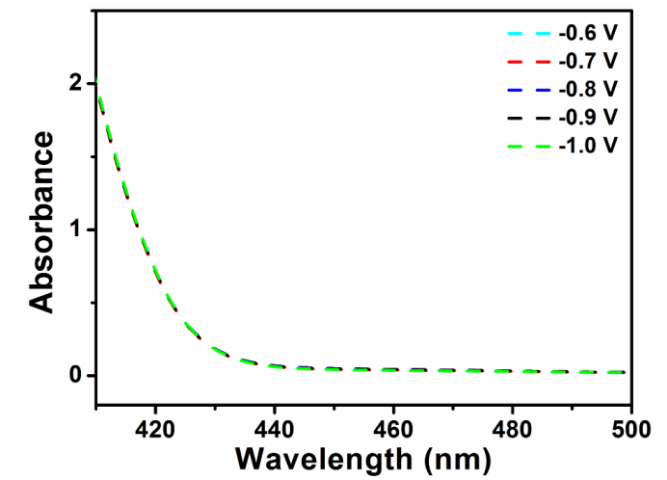

Fig. S8. UV-Vis absorption spectra of the electrolytes after NRR electrolysis at a series of potentials after incubated for 10 min at room temperature.

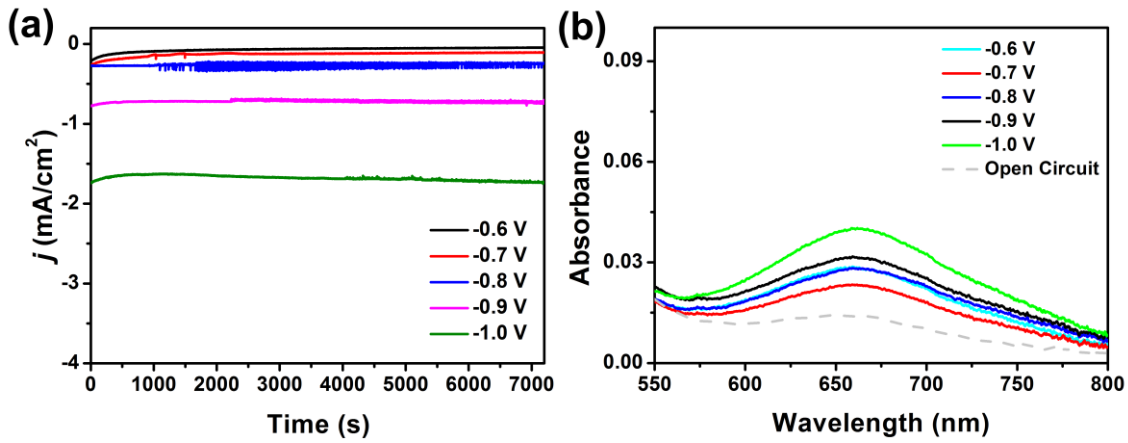

Fig. S9. (a) Time-dependent current density curves of CeO_2 at a series of potentials. (b) UV-Vis absorption spectra of the electrolytes stained with an NH_3 color agent after charging at different potentials for 2 h.

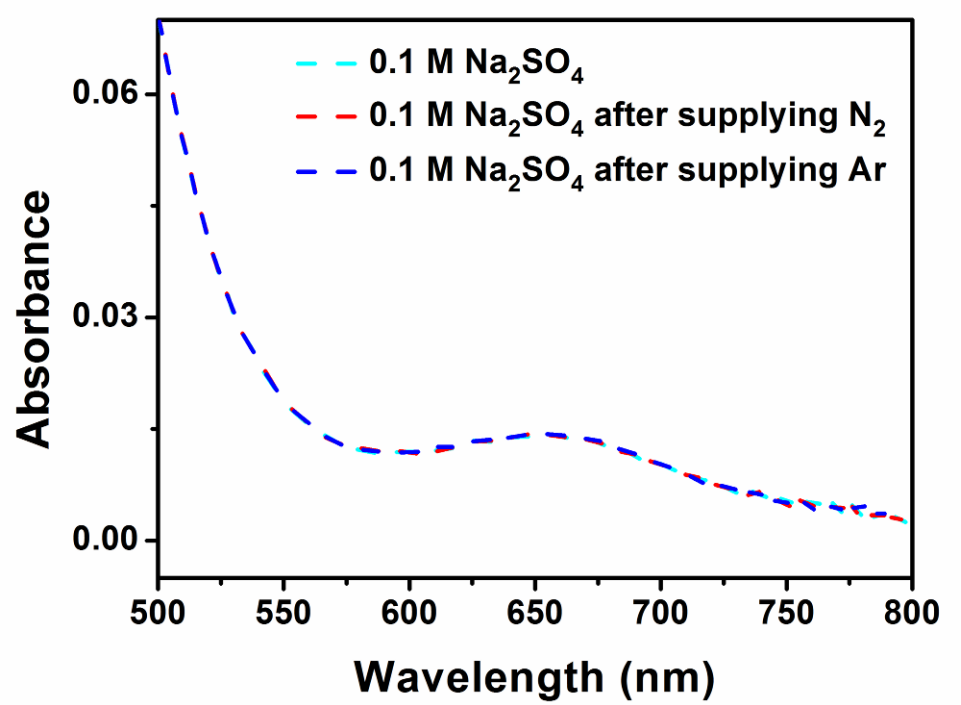

Fig. S10. UV-Vis absorption spectra of the 0.1 M Na_2SO_4 electrolyte stained with indophenol indicator after continuously supplying N_2 or Ar with no applied voltage

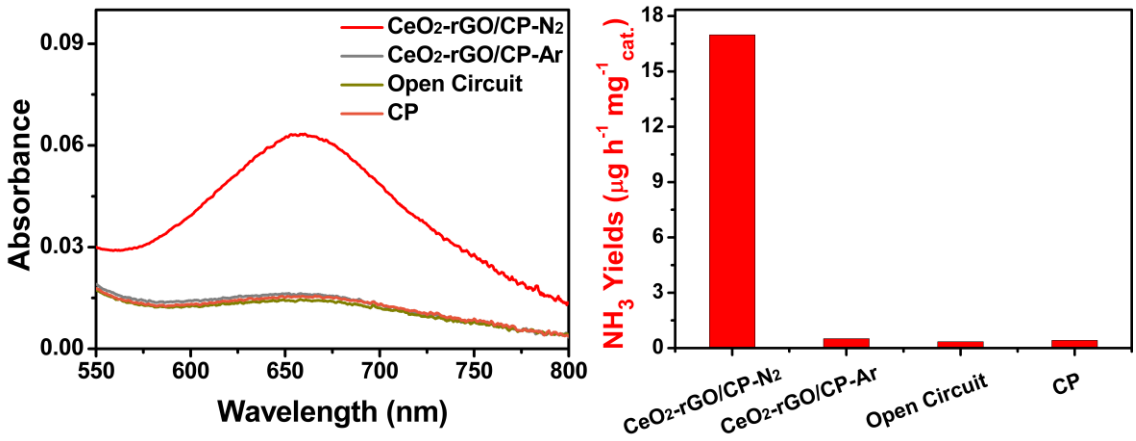

Fig. S11. The UV-Vis absorption spectra (left) and yield of NH_3 (right) at -0.7 V for 2 h under different electrochemical conditions.

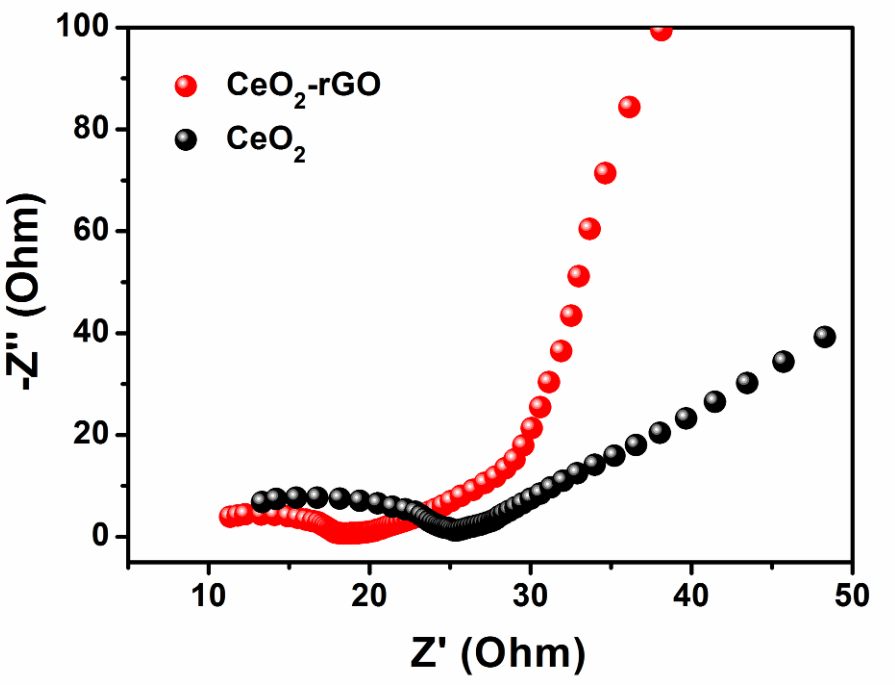

Fig. S12. (a) Nyquist plots of CeO_2–rGO/CP and CeO_2/CP

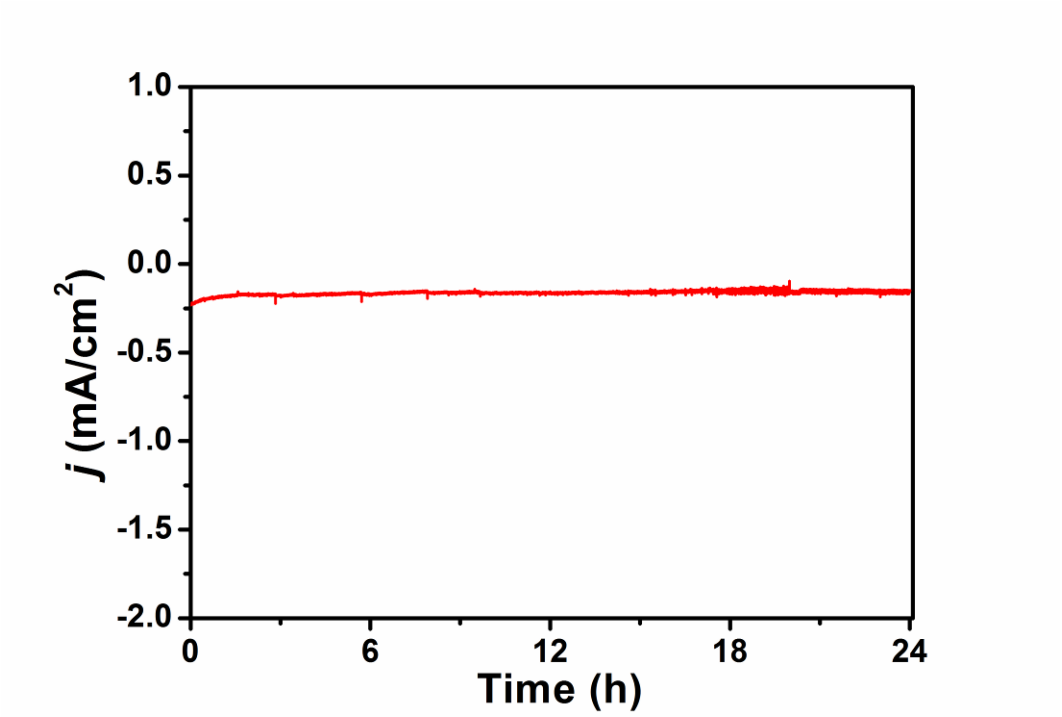

Fig. S13. Time-dependent current density curve for CeO_2-rGO/CP at the potential of –0.7 V for 24 h.

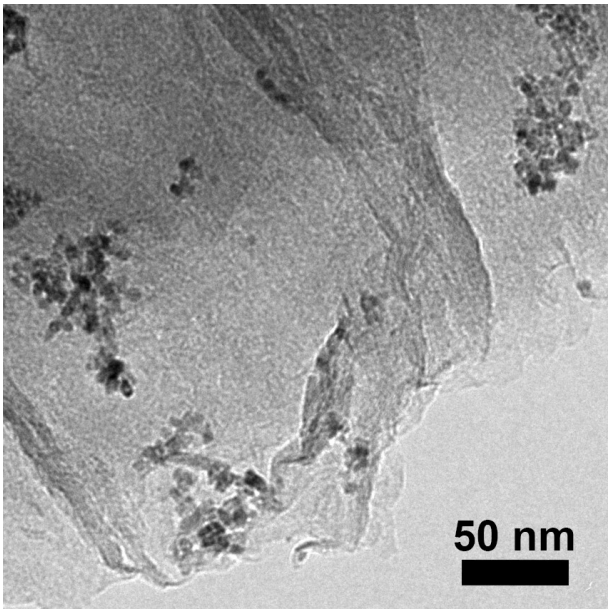

Fig. S14. TEM images of the CeO2-rGO after reaction.

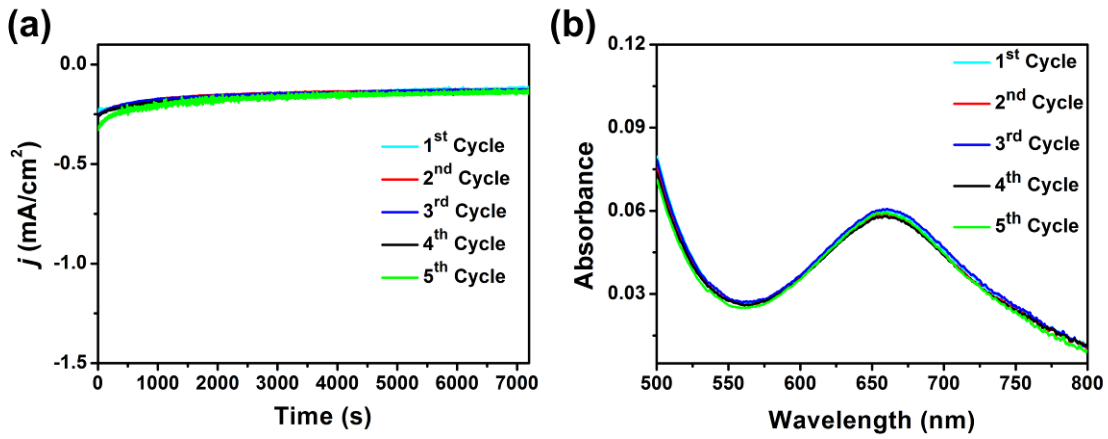

Fig. S15. (a) Time-dependent current density curves of CeO_2-rGO/CP at – 0.7 V for continuous cycles. (b) UV-Vis absorption spectra of the electrolytes stained with an NH_3 color agent for continuous cycles.

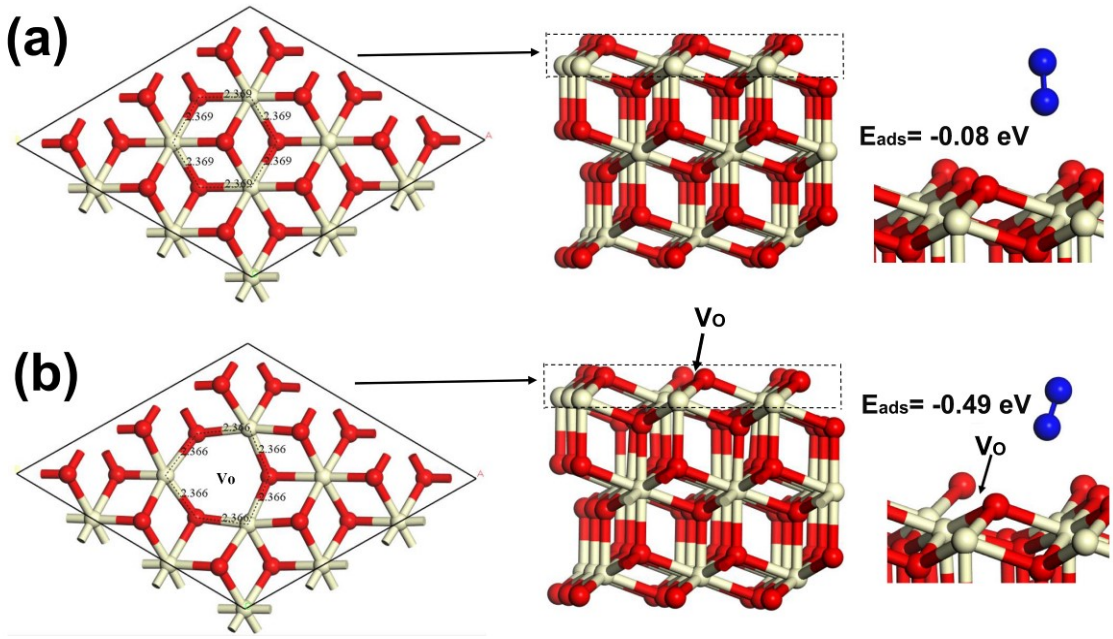

Fig. S16. The optimized adsorption configurations and its corresponding adsorption energy to N_2 of (a) CeO_2 (111) and (b) CeO_2 (111) with oxygen vacancy (V_O). [Legend: light yellow, Ce; red, O; and blue, N.]

Table S1. Comparison of the electrocatalytic NRR performance of CeO_2-rGO with other aqueous-based NRR electrocatalysts under neutral condition at room temperature.

Catalyst	Electrolyte	Potential	NH_3 yield	FE	Ref.
CeO_2-rGO	**0.1 M Na_2SO_4**	**−0.7 V**	**16.98 μg h^{-1} $mg^{-1}_{cat.}$**	**4.78%**	**This work**
$Cr_{0.1}CeO_2$	0.1 M Na_2SO_4	−0.7 V	16.8 μg h^{-1} $mg^{-1}_{cat.}$	3.87%	10
MoS_2/CC	0.1 M Na_2SO_4	−0.5 V	4.94 μg h^{-1} cm^{-2}	1.17%	11
TiO_2	0.1 M Na_2SO_4	−0.7 V	9.16×10^{-11} mol s^{-1} cm^{-2}	2.5%	12
PEBCD/C	0.5 M Li_2SO_4	−0.5 V	2.58×10^{-11} mol s^{-1} cm^{-2}	2.85%	13
Mn_3O_4 nanocube	0.1 M Na_2SO_4	−0.8 V	11.6 μg h^{-1} $mg^{-1}_{cat.}$	3.0%	14
Fe_2O_3 nanorods	0.1 M Na_2SO_4	−0.8 V	15.9 μg h^{-1} $mg^{-1}_{cat.}$	0.94%	15
Fe_3O_4/Ti	0.1 M Na_2SO_4	−0.4 V	5.6×10^{-11}mol s^{-1} cm^{-2}	2.6%	16
TiO_2-rGO	0.1 M Na_2SO_4	−0.9 V	15.13 μg h^{-1} $mg^{-1}_{cat.}$	3.3%	17
SnO_2	0.1 M Na_2SO_4	−0.7 V	1.47×10^{-10} mol s^{-1} cm^{-2}	2.17%	18
C-TiO2	0.1 M Na_2SO_4	−0.7 V	16.22 μg h^{-1} $mg^{-1}_{cat.}$	1.84%	19
B-TiO2	0.1 M Na_2SO_4	−0.8 V	14.4 μg h^{-1} $mg^{-1}_{cat.}$	3.4%	20
MnO	0.1 M Na_2SO_4	−0.39 V	1.11×10^{-10} mol s^{-1} cm^{-2}	8.02%	21
AuHNCs	0.5 M $LiClO_4$	−0.5 V	3.98 μg h^{-1} cm^{-2}	14.8%	22
Nb_2O_5 nanowires array/CC	0.1 M Na_2SO_4	−0.6 V	1.58×10^{-10} mol s^{-1} cm^{-2}	2.26%	23
porous bromide-derived Ag film	0.1 M Na_2SO_4	-	2.07×10^{-11} mol s^{-1} cm^{-2} (−0.6 V)	7.36% (−0.5 V)	24
S-doped carbon nanospheres	0.1 M Na_2SO_4	−0.7 V	19.07 μg h^{-1} $mg^{-1}_{cat.}$	7.47%	25

r-CeO2	0.1 M Na_2SO_4	-	16.4 μg h^{-1} $mg^{-1}_{cat.}$ (−0.5 V)	3.7% (−0.4 V)	26

Reference

1 D. Zhu, L. Zhang, R. E. Ruther and R. J. Hamers, *Nat. Mater.*, 2013, **12**, 836–841.

2 G. W. Watt and J. D. Chrisp, *Anal. Chem.*, 1952, **24**, 2006–2008.

3 G. Kresse and J. Hafner, *Phys. Rev. B*, 1993, **17**, 13115–13118.

4 G. Kresse and J. Hafner, *Phys. Rev. B*, 1994, **49**, 14251.

5 G. Kresse and J. Furthmüller, *Comp. Mater. Sci.*, 1996, **6**, 15–50.

6 M. Nolan, S. C. Parker and G. W. Watson, *Surf. Sci.*, 2005, **595**, 223–232.

7 M. Nolan, *J. Mater. Chem.*, 2011, **21**, 9160.

8 J. Wang and X. Q. Gong, *Appl. Surf. Sci.*, 2018, **428**, 377–384.

9 http://ccbdb.nist.gov/.

10 H. Xie, H. Wang, Q. Geng, Z. Xing, W. Wang, J. Chen, L. Ji, L. Chang, Z. Wang and J. Mao, *Inorg. Chem.*, 2019, **58**, 5423-5427.

11 L. Zhang, X. Ji, X. Ren, Y. Ma, X. Shi, Z. Tian, A. M. Asiri, L. Chen, B. Tang and X. Sun, *Adv. Mater.*, 2018, **30**, 1800191.

12 R. Zhang, X. Ren, X. Shi, F. Xie, B. Zheng, X. Guo and X. Sun, *ACS Appl. Mater. Interfaces,* 2018, **10**, 28251–28255.

13 G. Chen, X. Cao, S. Wu, X. Zeng, L. Ding, M. Zhu and H. Wang, *J. Am. Chem. Soc.*, 2017, **139**, 9771–9774.

14 X. Wu, L. Xia, Y. Wang, W. Lu, Q. Liu, X. Shi and X. Sun, *Small,* 2018, **14**, 1803111.

15 X. Xiang, Z. Wang, X. Shi, M. Fan and X. Sun, *ChemCatChem,* 2018, **20**, 4530–4535.

16 Q. Liu, X. Zhang, B. Zhang, Y. Luo, G. Cui, F. Xie and X. Sun, *Nanoscale,* 2018, **10**, 14386–14389.

17 X. Zhang, Q. Liu, X. Shi, A. M. Asiri, Y. Luo, X. Sun and T. Li, *J. Mater. Chem. A,* 2018, **6**, 17303–17306.

18 L. Zhang, X. Ren, Y. Luo, X. Shi, A. M. Asiri, T. Li and X. Sun, *Chem. Commun.* 2018, **54**, 12966–12969.

19 K. Jia, Y. Wang, Q. Pan, B. Zhong, Y. Luo, G. Cui, X. Guo and X. Sun, *Nanoscale Adv.*, 2019, **1**, 961-964.

20 Y. Wang, K. Jia, Q. Pan, Y. Xu, Q. Liu, G. Cui, X. Guo and X. Sun, *ACS Sustainable Chem. Eng.*, 2019, **7**, 117–122.

21 Z. Wang, F. Gong, L. Zhang, R. Wang, L. Ji, Q. Liu, Y. Luo, H. Guo, Y. Li, P. Gao, X. Shi, B. Li, B. Tang and X. Sun, *Adv. Sci.*, 2018, **5**, 1801182.

22 M. Nazemi, S. R. Panikkanvalappil and M. A. El-Sayed, *Nano Energy*, 2018, **49**, 316–323.

23 W. Kong, Z. Liu, J. Han, L. Xia, Y. Wang, Q. Liu, X. Shi, Y. Wu, Y. Xu and X. Sun, *Inorg. Chem. Front.*, 2019, **6**, 423–427.

24 L. Ji, X. Shi, A. M. Asiri, B. Zheng and X. Sun, *Inorg. Chem.*, 2018, **57**, 14692–14697.

25 L. Xia, X. Wu, Y. Wang, Z. Niu, Q. Liu, T. Li, X. Shi, A. M. Asiri and X. Sun, *Small Methods*, 2019, **3**, 1800251.

26 B. Xu, L. Xia, F. Zhou, R. Zhao, H. Chen, T. Wang, Q. Zhou, Q. Liu, G. Cui, X. Xiong, F. Gong and X. Sun, *ACS Sustainable Chem. Eng.* 2019, **7**, 2889–2893.